

Single-Layer Laser-Based Powder Bed Fusion of Lunar Regolith Simulants in Vacuum as a First Step to Direct Additive Manufacturing on the Moon

Tjorben Griemsmann¹ · Mathias Ernst¹ · Jan Perwas¹ · Tim Eismann¹ · Roland Kalms¹ · Nicole Emminghaus¹ · Peter Wessels¹ · Jörg Hermsdorf¹ · Julian Baasch² · Stefan Linke² · Enrico Stoll² · Jörg Neumann¹ · Stefan Kaierle^{1,3}

¹Laser Zentrum Hannover e.V., Hollerithallee 8, 30419 Hannover, Germany;

²Institute of Aeronautics and Astronautics, Technische Universität Berlin, Marchstraße 12-14, 10587 Berlin, Germany

³Institute of Transport and Automation Technology, Leibniz Universität Hannover, An der Universität 2, 30823 Garbsen, Germany

https://doi.org/10.58134/fh-aachen-rte_2024_013

Abstract

For the creation of lunar infrastructure, the utilization of locally available materials is essential, because transport from Earth is expensive. The lunar soil, or regolith, is widely spread above the surface of the Moon and represents a predestined construction material. The regolith is a fine-grained powder and processing it with powder-based additive manufacturing technologies is a promising approach since no special tools are needed to build various structures on the Moon. The powder bed fusion process should work directly in the lunar environment for building habitats, landing pads, and other infrastructure. The process must, therefore, work without the commonly used build platform and without a gas atmosphere. In this article, the first experiments of single-layer laser-based powder bed fusion of mare, highland, and an intermediate regolith simulant under vacuum and without a build platform are presented. The influence of the scanning speed, hatch distance, and scanning pattern on the surface quality is investigated. Low scanning speeds and hatch distances lead to smooth single-layers without irregularities. Chamber pressure recordings and Energy Dispersive X-ray spectroscopy (EDX) measurements show that constituents of the regolith simulants vaporize during the fusion process. The applicability for larger single-layers and multi-layer 3D structures is demonstrated as an outlook. The results represent the first step towards additive manufacturing on the Moon.

Keywords In-situ resource utilization · Lunar infrastructure · Vacuum · Lunar regolith · Laser-based powder bed fusion

1. Introduction and motivation

Sustainable and affordable solar system exploration requires the use of local materials, the so-called In Situ Resource Utilization (ISRU). The Moon is our nearest celestial body at a mean distance of 384.400 km. Therefore, it is the most obvious site to build expertise and skills in setting up an extraterrestrial base. Technologies and principles can afterward be applied to explore other celestial bodies like Mars. Almost the complete surface of the Moon is covered with fine-grained soil, the lunar regolith [1]. Among others, the European Space Agency (ESA) and National Aeronautics and Space Administration (NASA) issue the objective to develop technologies for processing the lunar regolith into propellants and life-supporting consumables like oxygen, but also for using it as a construction material [2, 3]. Additive manufacturing (AM) is predestined for construction on the

Moon since no special tools from Earth are needed for building individual construction parts or infrastructure of a lunar base. There are several investigations regarding AM of lunar regolith with technologies that need additional material like stereolithography [4, 5], ink-jetting [6, 7], or the D-Shape and Contour Crafting approach [8, 9]. These technologies have the potential to 3D-print lead-bearing parts but have the disadvantage that consumables from Earth or complex synthesis processes on the Moon are still needed. In the case of stereolithography and ink-jetting, additional sintering processes are necessary to produce dense parts and to remove the binder material [4, 5, 7]. AM processes that directly melt the regolith without additional material are also under investigation. The most researched technologies are selective solar sintering, where concentrated sunlight is used to melt the regolith [10, 11], and laser-based powder bed fusion (PBF-LB) [12–14]. Small construction parts can be manufactured with both technologies and

the size of the parts is conventionally limited by the build chamber of the machine. All processes reported were conducted in an air or gas atmosphere with ambient pressure, or in one case, with a low-pressure condition of 150 mbar [11]. All works were carried out using a build platform as a heat sink and to prevent warping effects.

However, the first applications on the Moon would concern building landing pads, habitats, and infrastructure for dust mitigation like streets [15]. The AM technology should therefore work directly on the lunar surface without special hardware and closed process chambers. This means, the process should work in a vacuum (approximately 10^{-12} mbar [1]) and without a build platform. The first single-layers manufactured with a PBF-LB similar process were recently reported [16–18], but the experiments were carried out in the Earth's atmosphere, and applicability on the lunar surface is uncertain.

This article deals with single-layer PBF-LB of lunar regolith simulants without a build platform and in a vacuum to close the above-described gap of knowledge. A laboratory setup consisting of a laser diode, galvanometer scanner, and vacuum chamber was developed. Process parameter studies with varying scanning speed, hatch distance, and scanning patterns were carried out for three different simulants with compositions of different regions of the Moon. The influence of the process parameters and simulant composition on the samples was determined. The investigations included measurement and description of process-induced changes in the pressure in the vacuum chamber and a visual inspection of the samples. The surface topography was measured using a laser scanning microscope. Energy Dispersive X-ray spectroscopy (EDX) was carried out to compare the elemental composition of the melted single-layer with the simulant composition. A scaling approach for large structures and a first double-layer are presented as an outlook. Finally, a conclusion and an outlook regarding future work are given.

2. Materials and methods

The used lunar regolith simulants and the experimental setup are described in this section. Furthermore, the experimental design and evaluation methods are explained.

2.1. Lunar regolith simulants

The composition of the lunar regolith varies in different regions of the Moon and, as a result, the PBF-LB process behavior could also change. To investigate the influence of the composition, three simulants – namely TUBS-M, TUBS-I, and TUBS-T [19] – were used in this work. These are basic lithic regolith simulants, representing the mare regions of the Moon with the basaltic TUBS-M and the highland regions with the anorthositic TUBS-T. TUBS-I is an intermediate version, where TUBS-M and TUBS-T are mixed in equal weight. The chemical composition is given in Table 1.

Table 1: Chemical composition of TUBS-M and TUBS-T from [19]

Compounds	TUBS-M in wt%	TUBS-T in wt%
SiO ₂	48.61	48.71
TiO ₂	2.29	0.12
Al ₂ O ₃	13.28	30.33
FeO	10.14	1.05
MgO	8.73	0.57
CaO	8.31	14.57
Na ₂ O	3.67	3.05
K ₂ O	1.71	0.22
MnO	0.18	0.02
Cr ₂ O ₃	0.04	-
P ₂ O ₅	0.51	-
Loss on ignition	0.63	0.99

The simulants were developed to imitate the real regolith and are not optimized in particle shape or size for powder bed fusion processes. A scanning electron microscopy (SEM) image of the TUBS-M powder is shown in Figure 1.

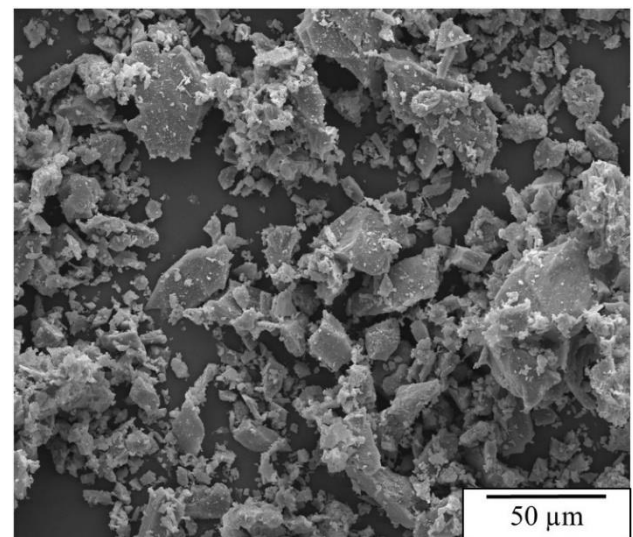


Figure 1: SEM image of sharp-edged lunar regolith simulant TUBS-M powder

The shape of the particles is sharp-edged, and the particle size ranges between 10 μm and 2 mm according to the manufacturer's information. Details about the simulants can be found in [19].

2.2. Experimental setup

A laboratory setup for single-layer PBF-LB was developed to perform the melting process in a vacuum chamber. The setup, shown in Figure 2, consists of a diode laser (element e12, nLIGHT) with a maximum power output of 150 W at a wavelength centroid of 976 nm guided in an optical fiber with a 105 μm core diameter and a numerical aperture of 0.22. A diode laser was chosen because of its high wall-plug efficiency, robustness, and compact design as well as space qualification and test programs [20], considering a future lunar mission.

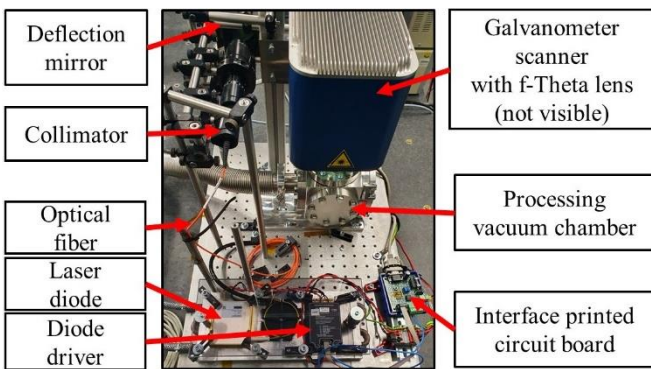


Figure 2: Experimental setup for single-layer PBF-LB of lunar regolith simulants in vacuum

The laser diode is controlled by a diode driver (Fast Modulator MSM 20-50, MESSTEC Power Converter GmbH) and a custom printed circuit board to convert the signals of the scanner control board (RTC4, SCANLAB GmbH). The output beam of the fiber is collimated via an aspherical lens (AHL18-15, Asphericon GmbH) and guided to the galvanometer scanner (Rhino 30, Arges GmbH) via two mirrors. The laser beam is focused by an f-Theta lens (S4LFT2163/094, Sill Optics GmbH & Co. KG) with a focal length of 162 mm. Scanning paths, scanning speed, and laser power are set and commanded to the scanner control board via a Python script. The laser beam is guided into a vacuum chamber through an exchangeable anti-reflective coated fused silica window. The powder bed container with a cuboid powder bed size of 38 mm \times 38 mm \times 8 mm (w \times l \times h) can be inserted through a quick access door. The chamber is evacuated by using a vacuum pump (TSH 071 E, Pfeiffer Vacuum GmbH), and the pressure is measured with a digital gauge (PPT 200, Pfeiffer Vacuum GmbH).

The laser beam caustic was measured with a focus monitor device (DFIG-PS, Primes GmbH) before starting the

experiments and is plotted in Figure 3a. The beam diameter in the working plane is 1.9 mm (beam width definition to an intensity of $1/e^2$). The working plane was chosen to be above the actual focal plane to achieve a more homogenous intensity profile of the laser beam. The actual intensity profile of the laser beam is given in Figure 3b.

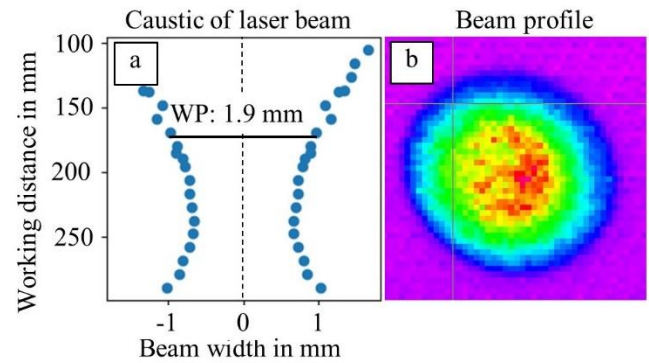


Figure 3: (a) Caustic measurement of the laser beam (beam width definition to an intensity of $1/e^2$), working distance related to f-Theta lens; (b) intensity profile of the laser beam in working plane (WP)

2.3. Experimental methods

The real lunar regolith does not contain moisture or crystalline water (except in the areas around the poles). To remove this water from the simulants before the experiments the powder was heated up to 700 $^{\circ}\text{C}$ with a dwell time of four hours in an oven in ambient atmosphere. After cooling, the simulant was stored in sealed bottles until usage. Each single-layer PBF-LB experiment was performed in the same manner. The powder bed was filled with regolith simulant and leveled by wiping off the oversupplied material with a metal sheet. The powder bed container was inserted into the vacuum chamber and then evacuated to a maximum pressure level of $2.2 \cdot 10^{-2}$ mbar. The recordings of the pressure and the laser process were started, while the vacuum pump was kept running. When the melting of the layer was finished, the vacuum pump was turned off and air was let into the vacuum chamber. The sample was extracted up from the powder bed, and the adhered powder was wiped off with a brush.

The nominal shape of the manufactured single-layers was a square with an edge length of 20 mm. The investigated process parameters with the chosen levels are given in Table 2. The chosen experimental design was full factorial, so every possible process parameter combination was tested. The experiments were carried out for each of the three simulants and repeated once if the first sample was not completely broken.

Table 2: Full factorial experimental design for process parameter tuning; the laser power was fixed to 60 W

Process parameter	Values/condition
Hatch distance h in mm	1, 1.5, 2
Scanning speed v in mm/s	2, 3, 4
Scanning pattern	Consecutive, reordered, contour filling
Powder bed compression	Compressed, loose

The scanning speed, hatch distance, and laser power (fixed to 60 W) values were based on pre-trials for single melt tracks [21]. The three investigated scanning patterns are schematically illustrated in Figure 4. In Figure 4a, the scanning paths are consecutively ordered and unidirectional. Figure 4b shows a reordered version of the unidirectional scanning paths. This was done to distribute the heat input more homogeneously and to avoid heat accumulation since the thermal conductivity through the powder bed is expected to be below $10^{-1} \text{ W m}^{-1}\text{K}^{-1}$ [22]. The scanning pattern of Figure 4c is based on a contour filling pattern of common PBF-LB processes. The scan paths are ordered from the inside to the outside to avoid heat accumulation in the middle of the single-layer. In all patterns, a pause of 10 seconds was introduced after each scan path to avoid overheating. The powder bed compression condition “loose” means that the simulant was only poured into the powder bed container and leveled. The condition “compressed” means that the powder was compacted by manually pressing a stamp with the size of the powder bed onto the powder without controlled force.

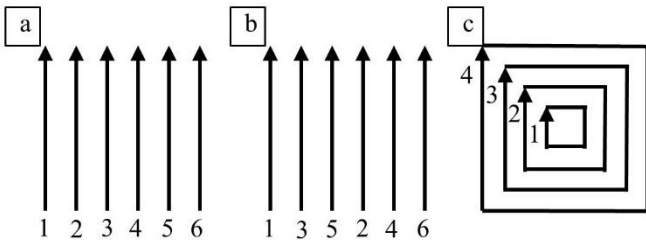


Figure 4: Schematic illustration of investigated scanning patterns, scanning paths are numbered consecutively; (a) consecutive, (b) reordered, and (c) contour filling

Following the completion of the process parameter study, a scaling approach was undertaken to produce larger single-layer samples. Therefore, the most promising process parameter combination for a smooth surface (smallest maximum height difference on the upper surface of the sample) was chosen for each simulant, and a larger single-layer was manufactured by placing four squares next to each other in a way that they are melted together. Each square was rotated about 90° like a common PBF-LB chessboard pattern. A first demonstration

of multi-layer PBF-LB was performed by manually covering one manufactured single-layer with regolith simulant powder. The powder layer thickness of 3 mm for the second layer was chosen according to the thickness of the single-layer and the difference to the powder bed container height. Both layers were manufactured with the same process parameters as for the above-described larger single-layer.

2.4. Analytic methods

The first analysis carried out with every manufactured single-layer was a visual inspection to check if all melt tracks were fully connected. Single-layers, which were broken or consisted of several parts, were not analyzed further. Images of the samples were taken and compared for the different used simulants and process parameters. The surface profile of the manufactured single-layers was measured using a laser scanning microscope (VK-X1000, Keyence) in reflected light mode. Based on the measurements the highest difference from the global minimum to the maximum was determined. The recordings of the pressure sensor connected to the vacuum chamber were plotted and compared to achieve a better understanding of the process. Additionally, EDX measurements were taken with a Quanta 400 FEG (FEI Thermo Fisher Scientific) scanning electron microscope to compare the elemental composition of the raw simulant, the melted material, and the condensates in the vacuum chamber.

3. Results and discussion

The following section presents and discusses the results of the single-layer PBF-LB experiments.

3.1. Visual comparison of single-layers

The first results of single-layer PBF-LB experiments showed that the “reordered” scanning pattern has disadvantages compared to the “consecutive” pattern.

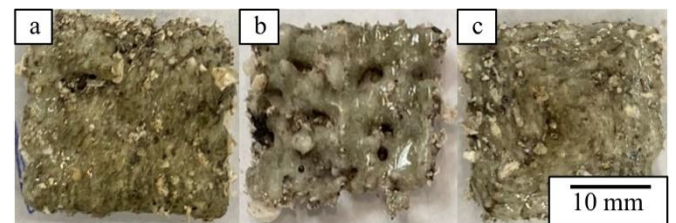


Figure 5: Comparison of samples manufactured with different scanning patterns: (a) “consecutive”, (b) “reordered”, (c) “contour filling”; samples manufactured with TUBS-T, $h = 1 \text{ mm}$, and $v = 2 \text{ mm/s}$

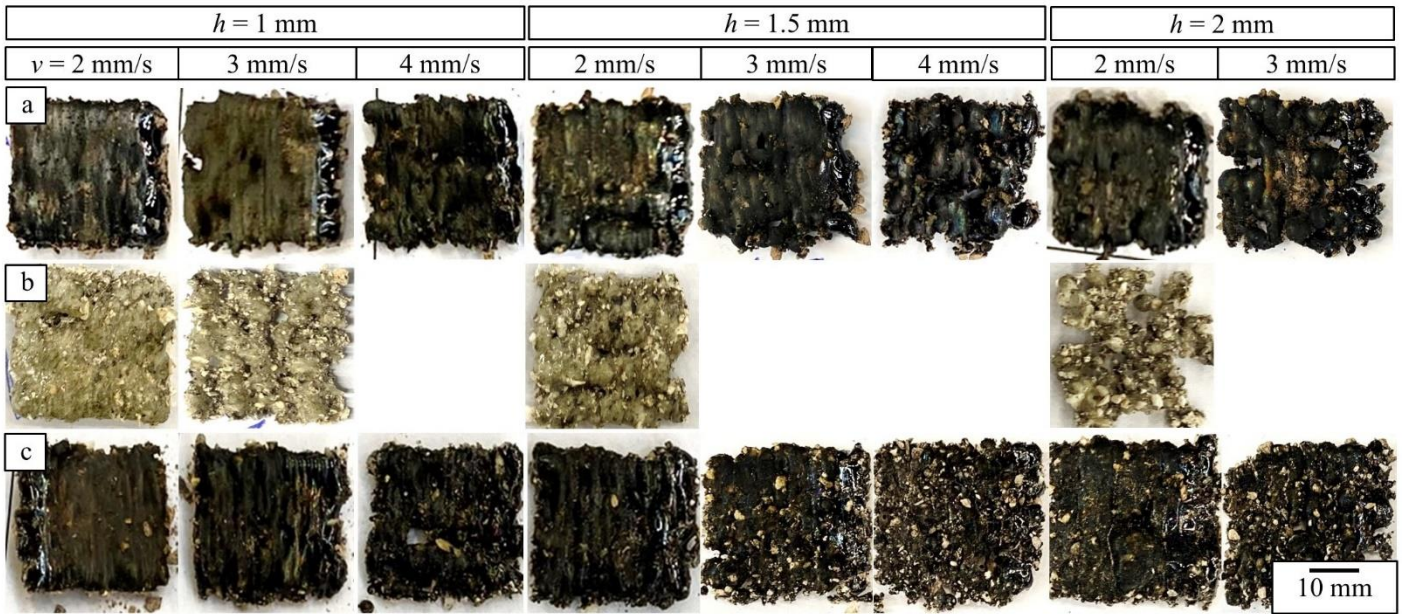


Figure 6: Results of single-layer PBF-LB with compressed powder and "consecutive" scanning pattern; (a) TUBS-M, (b) TUBS-T and (c) TUBS-I

Figure 5 illustrates an example of three single-layers manufactured out of TUBS-T.

One was manufactured with the "consecutive" (Figure 5a), one with the "reordered" (Figure 5b), and one with the "contour filling" (Figure 5c) pattern. While the "consecutive" and "contour filling" scanning pattern resulted in a relatively smooth and closed single-layer surface, the single-layer with a "reordered" scanning pattern showed valleys and holes. The borders of this single-layer were also more frayed. The assumed reasons are that several scanning vectors are created without contact with already molten material during manufacturing according to the "reordered" pattern. This leads to a lower heat conductivity and, therefore, the melt stays longer in the liquid phase and surface tension effects, like balling, occur. The described behaviour occurs for all investigated process parameter combinations, therefore the "reordered" scanning pattern was discarded at an early stage of the experiments.

Figure 6 shows an image comparison of the single-layers manufactured with compressed powder and a "consecutive" scanning pattern for all three regolith simulants. TUBS-M Figure 6a) and TUBS-I (Figure 6c) could be successfully processed with all investigated scanning speeds and hatch distances except 4 mm/s scanning speed and 2 mm hatch distance. TUBS-T (Figure 6b) was only successfully processable with 2 mm/s scanning speed in all tested hatch distances and 3 mm/s for a hatch distance of 1 mm. The other process parameter combinations led to unconnected melt beads in the powder bed. Regarding the general dependence on the scanning speed and the hatch distance, all simulants showed a similar behaviour. The single-layer surfaces are

smoother and less interrupted for lower scanning speeds, lower hatch distances, and, therefore, higher average energy densities and overlaps of melt tracks. The worse processability of TUBS-T could be explained by a higher melting point of the components [23]. Visual differences of PBF-LB single-layers manufactured from loose or compressed powder were not noticeable (see Figure 7).

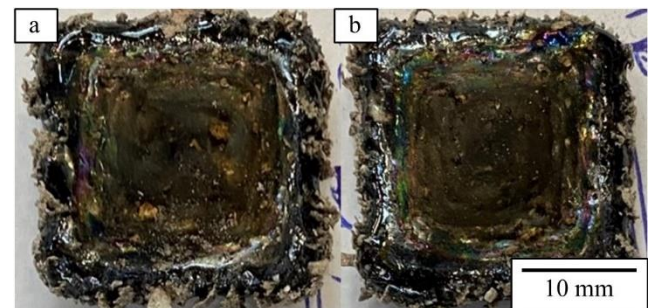


Figure 7: Comparison of TUBS-I samples with "contour filling" pattern, $v = 2 \text{ mm/s}$ and $h = 1 \text{ mm}$; (a) "loose" and (b) "compressed" powder bed condition

The thickness of the single-layers was approximately 5 mm with a very rough down skin surface, which made exact measurements difficult. Examples of the measured surface profiles of the single layers are given in Figure 8 for different PBF-LB process parameters. The first column of Figure 8 represents the single-layers manufactured with the highest energy density for the three different simulant types. The TUBS-M sample shows the smoothest surface with the lowest height difference from the lowest to the highest point (2.0 mm). The TUBS-T sample has the highest height difference (3.1 mm) and a more irregular surface profile.

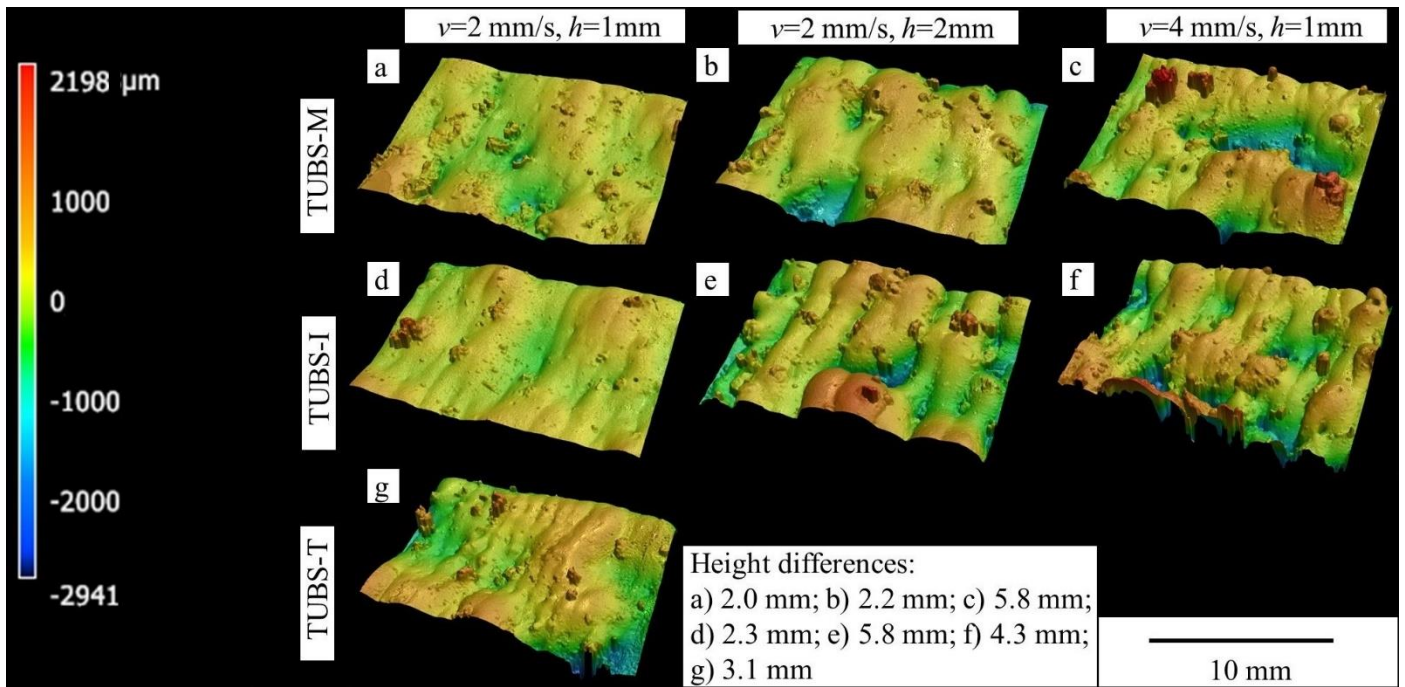


Figure 8: Surface profiles measured with reflective light mode of a laser scanning microscope; the height differences describe the distance from the minimum to the maximum point

The sample of the intermediate TUBS-I simulant is with 2.3 mm between the pure mare and highland simulants, as expected. However, the height profile of TUBS-I is more like TUBS-M than TUBS-T. This and the same number of applicable PBF-LB process parameter combinations for the creation of closed single-layers lead to the conclusion that TUBS-M is dominant over TUBS-T in the PBF-LB process behavior of regolith mixtures. The second column shows the surface profiles for the highest hatch distance and lowest scanning speed. The profiles are more irregular, and some melt tracks are interrupted. The maximum height difference is increased compared to column one. This is because using higher hatch distances leads to less overlap of the neighboring melt tracks and less remelting, which smoothes the surface, is applied. The third column represents the highest scanning speed with the lowest hatch distance. The height difference increases compared to column one as well. The reason is that at higher scanning speeds the melt pool is elongated, and balling effects occur because of the surface tension and low wettability of the underneath powder bed [24].

3.2. Pressure and EDX measurements

In Figure 9, typical plots of pressure measurements during the single-layer PBF-LB process are given. Before processing, the pressure was decreased below 0.018 mbar. When the laser beam was switched on, the pressure increased to approx. 0.030 mbar for TUBS-M, 0.024 mbar for TUBS-I, and 0.019 mbar for TUBS-T until the laser beam was switched off after ten seconds.

In the dwell time between two scanning tracks, the pressure was decreased again because of the continuously running vacuum pump. The pressure increase during the laser melting is most probably caused by vaporizing constituents with low boiling or decomposition temperatures in the regolith simulants. Consequently, the different pressure increases for the three simulants are caused by the different material compositions. While laser beam melting of TUBS-M increases the pressure the most, laser beam melting of TUBS-T has the smallest effect on the pressure. Laser beam melting of TUBS-I, the intermediate simulant, has an intermediate effect on the pressure.

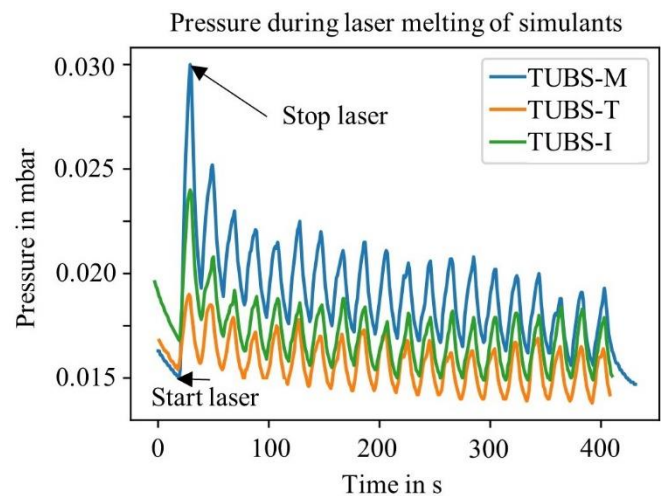


Figure 9: Pressure recording in the vacuum chamber during single-layer PBF-LB of different regolith simulants

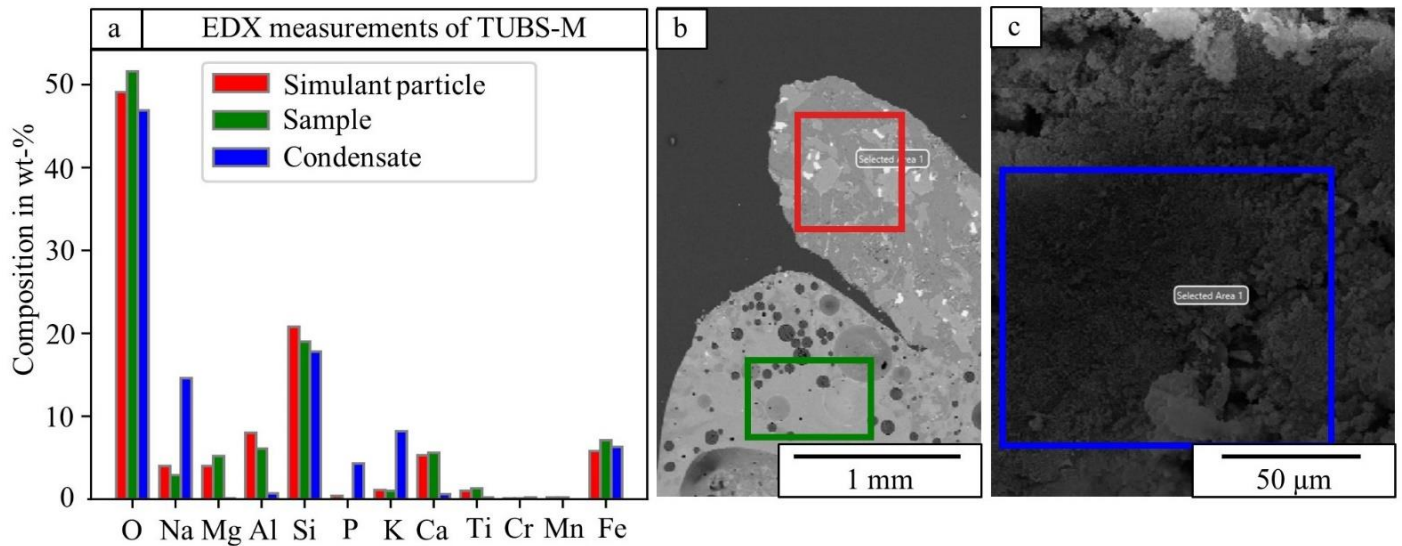


Figure 10: EDX measurements of TUBS-M particle, sample, and condensate collected in the vacuum chamber after the PBF-LB process; (a) comparison of the compositions in weight percent; (b) locations of the measurements in SEM image of a particle (red rectangle) and the laser melted sample (green); (c) SEM image with measuring area of condensate in the vacuum chamber (blue)

For all simulants, the first laser scan track creates the highest increase in pressure. This is because the first line is directly scanned into the powder bed and there is no remelting of a previous track. There is less vaporization in already melted scanning tracks because constituents are already vaporized. This explanation can be confirmed by inspecting a pressure record of a sample with the “reordered” scanning pattern. For a hatch distance of 1 mm seven peaks with high, seven peaks with medium, and six peaks with low pressure increase can be found. The first group of peaks is related to the scan tracks which only melt unsolidified powder, the second group of peaks is related to scan tracks with solidified melt on one side, and the last group is related to the scanning tracks in between with almost only solidified melt.

The surface of the vacuum chamber was covered with a white deposit after the PBF-LB process. EDX measurements of the white deposit were performed to investigate the constituents of the deposit. The measurements were compared to an unmolten particle and the melted single-layer to confirm that the condensates are constituents that vaporize at low temperatures. The elemental compositions are illustrated in Figure 10a, and the SEM images in Figure 10b and c. The EDX measurements show that the white deposit mainly consists of compounds of elements with low boiling temperatures like sodium, potassium, and phosphorus. The proportion of these elements in the sample is reduced compared to the unmolten particle. Elements whose compounds tend to have a higher boiling temperature, like magnesium, aluminum, calcium, and titanium, were nearly not present in the white deposit. The EDX measurements also explain the lower pressure increase during laser melting of TUBS-T, because the percentage of sodium, potassium,

and phosphorus containing compounds is lower in contrast to TUBS-M [19]. It can be concluded that constituents with low boiling points contributed to the pressure increase during PBF-LB of the regolith simulants. Real lunar regolith has lower contents of sodium-, potassium-, and phosphorus-based compounds as shown in Table 3. Due to this different composition, vaporizing effects may differ for laser melting of real lunar regolith.

Table 3: Comparison of sodium, potassium, and phosphorus-based compounds of real regolith (average values from [19] based on [1, 25]) and used simulants ([19])

Compound in wt%	Basalts		Anorthosite	
	Real	TUBS-M	Real	TUBS-T
Na ₂ O	0.39	3.67	0.08	3.05
K ₂ O	0.06	1.71	0.01	0.22
P ₂ O ₃	0.07	0.51	-	-

3.3. Scalability and double-layer PBF-LB

AM of lunar infrastructure requires the possibility to manufacture large structures. One approach is to combine small structures, in this case squares, into larger single-layers. The four squares were placed in a chessboard pattern with a 90° rotated scanning direction. To demonstrate this approach, the process parameter combination that produced the smoothest surface of the PBF-LB single-layers was chosen. The large single-layers were manufactured with a “consecutive” scanning pattern, 1 mm hatch distance, and 2 mm/s scanning speed with compressed simulant powder. The results are illustrated in Figure 11. The large single-layers manufactured from all three regolith simulants all have a closed surface.

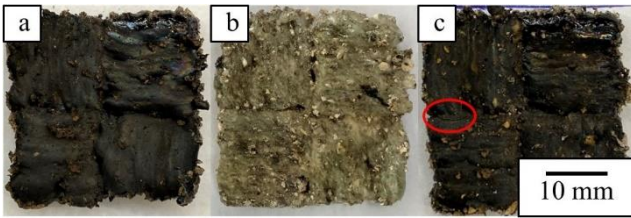


Figure 11: Images of connected small PBF-LB single-layers for scaling purposes; (a) TUBS-M, (b) TUBS-T, and (c) TUBS-I; the red ellipse indicates a crack

Only one crack was found in the connection of two squares made from TUBS-I, as indicated in Figure 11c. With these single-layers the two-dimensional scalability was demonstrated but three-dimensional infrastructure requires a PBF-LB process with the possibility to produce multiple-layers. As a first demonstration, a double-layer structure was manufactured from TUBS-I ($h = 1$ mm, $v = 2$ mm/s, “contour filling” pattern, 3 mm layer thickness) and is shown in Figure 12a. Figure 12b shows a cross-section of the layer interface and the internal structure.

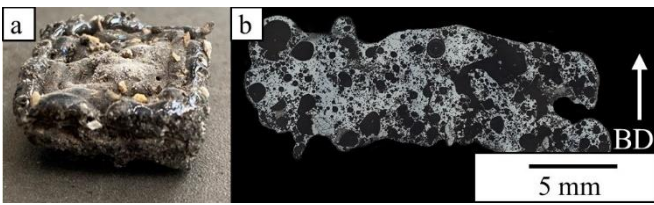


Figure 12: First manufactured double-layer sample from TUBS-I; (a) overview image, (b) cross-section of the layer interface with indicated build direction (BD)

The cross-section reveals that no cracks were created and a porosity of approximately 61 %. This is higher than the porosities reported by Farries et al. for regolith simulant laser beam melted in ambient air. Porosities ranged from 50 to 10 % depending on the regolith simulant [16]. Most of the pores in the double-layer are spherical, which indicates gas porosity [26]. This confirms that the origin of the previously described pressure increase is due to the evaporation of low boiling point constituents. Trapped gases in the powder bed can be excluded as a reason, because of the low ambient pressure in the build chamber. The two layers are completely fused, and no gap is visible. Also, the distribution of porosity is homogeneous. This double-layer structure demonstrates that PBF-LB of lunar regolith simulant in a vacuum and without build platform is possible.

4. Conclusion and outlook

In this article, single-layer PBF-LB of lunar regolith simulants in a vacuum and without a build platform was presented to simulate the environmental aspects on the

lunar surface. A custom experimental setup was developed to enable a vacuum in the build chamber. A compact laser diode was chosen as a laser beam source to take robustness as well as power efficiency and volume limitations for future space missions into account. The laser power was fixed to 60 W, and the process parameters hatch distance, scanning speed, scanning pattern, and powder compression were varied in a full factorial design. While the variation in powder compression showed no noticeable difference in the results, the surface of the single-layers was smoother and closed for lower scanning speeds and hatch distances. The “consecutive” unidirectional and “contour filling” scanning patterns led to fewer broken and less perforated melted layers than the “reordered” unidirectional scanning pattern. TUBS-M and TUBS-I were processable to complete layers with all investigated process parameter combinations except for 4 mm/s scanning speed and 2 mm hatch distance. TUBS-T needed lower scanning speeds and hatch distances to be melted to a complete layer ($v = 2$ mm/3 mm, $h = 1$ mm; $v = 2$ mm/s, $h = 1.5$ mm).

The pressure in the vacuum chamber increased during the PBF-LB process. The main reason is the vaporization of constituents with low boiling points or low decomposition temperatures. This statement is supported by EDX measurements of the original simulant powder, a melted sample, and white condensates found in the vacuum chamber. Other reasons, which are not known yet, are also possible to contribute to the high porosity.

A first scalability approach for large single-layers was demonstrated with all three regolith simulants. Transferability to real AM processes was proven by successfully manufacturing two layers on top of each other. By this, the presented work represents a first step in enabling direct AM on the Moon.

Based on the given results, future experimental setups and work should address the production of large crack-free layers and a possibility of automated recoating with a new layer of lunar regolith. A mechanism that avoids relative movement of the first layer during recoating should be developed. The applicability of the process in even higher vacuum environments should be investigated since the ambient pressure at the lunar surface is approximately 10^{-12} mbar [1]. Mechanical properties of the fused samples need to be characterized for the reliable construction of lunar infrastructure and strategies for lower porosity should be evaluated. The thermal insulation and radiation shielding properties should also be determined to qualify the PBF-LB processed regolith for human shelters on the Moon.

Since the work reported in this article was performed with an early-stage laboratory setup, hardware for direct PBF-LB on the lunar surface should be developed, like the payload described in [27]. Also, mechanisms for de-

fined recoating on the Moon would be needed. In the future, direct PBF-LB of lunar regolith may have an important role in creating solidified areas for dust control purposes, large landing pads, streets, or even habitats on the lunar surface.

5. Acknowledgement

The authors express their sincere thanks to the European Space Agency (ESA) for supporting the research in this publication under contract No 4000134975/21/NL/GLC/kk.

6. Contributions

Tjorben Griemsmann: Conceptualisation, investigation, interpretation, visualization, writing – original draft

Mathias Ernst: Development of experimental setup – hardware, writing – review and editing

Jan Perwas: Development of experimental setup – software and electronics, writing – review and editing

Tim Eismann: Writing – review and editing

Roland Kalms: Writing – review and editing

Nicole Emminghaus: Writing - review and editing

Peter Wessels: Conceptualisation, funding acquisition, writing – review and editing

Jörg Hermsdorf: Writing - review and editing

Julian Baasch: Resources, writing – review and editing

Stefan Linke: Conceptualisation, funding acquisition, writing – review and editing

Enrico Stoll: Supervision, writing – review and editing

Jörg Neumann: Conceptualisation, supervision, funding acquisition, writing – review and editing

Stefan Kaierle: Supervision, conceptualisation, writing – review and editing

References

1. Heiken G, Vaniman D, French BM, Schmitt J (1991) Lunar Sourcebook: A User's Guide to the Moon. Cambridge University Press
2. ESA (2019) ESA Space Resources Strategy. <http://exploration.esa.int/moon/61369-esa-space-resources-strategy/>. Accessed on 2023-12-20
3. National Aeronautics and Space Administration (NASA) (2016) Next Space Technologies for Exploration Partnerships -2. In: Broad Agency Announcement NNH16ZCQ001K. https://www.nasa.gov/sites/default/files/atoms/files/nextstep-2_omnibus_baa_amendment_22_2022-12-06.pdf. Accessed on 2023-06-10
4. Liu M, Tang W, Duan W, et al (2019) Digital light processing of lunar regolith structures with high mechanical properties. *Ceramics International* 45:5829–5836. <https://doi.org/10.1016/j.ceramint.2018.12.049>
5. Dou R, Tang WZ, Wang L, et al (2019) Sintering of lunar regolith structures fabricated via digital light processing. *Ceramics International* 45:17210–17215. <https://doi.org/10.1016/j.ceramint.2019.05.276>
6. Jakus AE, Koube KD, Geisendorfer NR, Shah RN (2017) Robust and Elastic Lunar and Martian Structures from 3D-Printed Regolith Inks. *Scientific Reports* 7:44931. <https://doi.org/10.1038/srep44931>
7. Taylor SL, Jakus AE, Koube KD, et al (2018) Sintering of micro-trusses created by extrusion-3D-printing of lunar regolith inks. *Acta Astronautica* 143:1–8. <https://doi.org/10.1016/j.actaastro.2017.11.005>
8. Cesaretti G, Dini E, De Kestelier X, et al (2014) Building components for an outpost on the Lunar soil by means of a novel 3D printing technology. *Acta Astronautica* 93:430–450. <https://doi.org/10.1016/j.actaastro.2013.07.034>
9. Khoshnevis B, Bodiford M, Burks K, et al (2005) Lunar Contour Crafting - A Novel Technique for ISRU-Based Habitat Development. In: 43rd AIAA Aerospace Sciences Meeting and Exhibit. American Institute of Aeronautics and Astronautics, Reston, Virginia, pp 7397–7409
10. Meurisse A, Makaya A, Willsch C, Sperl M (2018) Solar 3D printing of lunar regolith. *Acta Astronautica* 152:800–810. <https://doi.org/10.1016/j.actaastro.2018.06.063>
11. Fateri M, Meurisse A, Sperl M, et al (2019) Solar Sintering for Lunar Additive Manufacturing. *Journal of Aerospace Engineering* 32:04019101. [https://doi.org/10.1061/\(ASCE\)AS.1943-5525.0001093](https://doi.org/10.1061/(ASCE)AS.1943-5525.0001093)
12. Fateri M, Gebhardt A, Gabrielli RA, et al (2015) Additive manufacturing of lunar regolith for extra-terrestrial industry plant. In: Proc., 30th Int. Symp. on Space Technology and Science
13. Goulas A, Binner JGP, Engstrøm DS, et al (2019) Mechanical behaviour of additively manufactured lunar regolith simulant components. *Proceedings of the Institution of Mechanical Engineers, Part L: Journal of Materials: Design and Applications* 233:1629–1644. <https://doi.org/10.1177/1464420718777932>
14. Caprio L, Demir AG, Previtali B, Colosimo BM (2020) Determining the feasible conditions for processing lunar regolith simulant via laser powder bed fusion. *Additive Manufacturing*

- 32:101029.
<https://doi.org/10.1016/j.addma.2019.101029>
15. National Aeronautics and Space Administration (NASA) (2020) Lunar Surface Innovation Initiative.
https://www.nasa.gov/directorates/spacetech/Lunar_Surface_Innovation_Initiative. Accessed 22 Sep 2023
 16. Farries KW, Visintin P, Smith ST (2022) Direct laser sintering for lunar dust control: An experimental study of the effect of simulat mineralogy and process parameters on product strength and scalability. *Construction and Building Materials* 354:129191.
<https://doi.org/10.1016/j.conbuildmat.2022.129191>
 17. Linke S, Voß A, Ernst M, et al (2021) Two-Dimensional Laser Melting of Lunar Regolith Simulant Using the MOONRISE Payload on a Mobile Manipulator. *3D Printing and Additive Manufacturing*.
<https://doi.org/10.1089/3dp.2020.0323>
 18. Ginés-Palomares J-C, Fateri M, Kalhöfer E, et al (2023) Laser melting manufacturing of large elements of lunar regolith simulant for paving on the Moon. *Scientific Reports* 13:15593.
<https://doi.org/10.1038/s41598-023-42008-1>
 19. Linke S, Windisch L, Kueter N, et al (2020) TUBS-M and TUBS-T based modular Regolith Simulant System for the support of lunar ISRU activities. *Planetary and Space Science* 180:104747.
<https://doi.org/https://doi.org/10.1016/j.pss.2019.104747>
 20. Ott M, Eegholm N, Stephen M, et al (2006) NASA Parts and Packaging Program: High Power Laser Diode Array Qualification and Guidelines for Space Flight Environments. NASA Technical Reports 1–44
 21. Eismann T, Griemsmann T, Ernst M, et al (2023) Entwicklung von Prozessparametereinstellungen für das Laserstrahlschmelzen von Regolith unter Vakuum. In: Tagungsband 5. Niedersächsisches Symposium Materialtechnik. Clausthal
 22. Horai K (1981) The effect of interstitial gaseous pressure on the thermal conductivity of a simulated Apollo 12 lunar soil sample. *Physics of the Earth and Planetary Interiors* 27:60–71.
[https://doi.org/10.1016/0031-9201\(81\)90087-X](https://doi.org/10.1016/0031-9201(81)90087-X)
 23. Linke S (2022) Mechanische Werkstoffeigenschaften von lasergeschmolzenem lunarem Regolith Stefan Linke, Doctoral thesis, Technische Universität Braunschweig
 24. Gunenthiram V, Peyre P, Schneider M, et al (2018) Experimental analysis of spatter generation and melt-pool behavior during the powder bed laser beam melting process. *Journal of Materials Processing Technology* 251:376–386.
<https://doi.org/10.1016/j.jmatprotec.2017.08.012>
 25. Sibille L, Carpenter P, Schlagheck R, French R (2006) Lunar Regolith Simulant Materials: Recommendations for Standardization, Production, and Usage. NASA Technical Paper 142.
<https://doi.org/https://ntrs.nasa.gov/citations/20060051776>
 26. Emminghaus N, Paul J, Hoff C, et al (2022) Development of an empirical process model for adjusted porosity in laser-based powder bed fusion of Ti-6Al-4V. *The International Journal of Advanced Manufacturing Technology* 118:1239–1254. <https://doi.org/10.1007/s00170-021-07847-0>
 27. Neumann J, Ernst M, Taschner P, et al (2023) The MOONRISE-payload as proof of principle for mobile selective laser melting of lunar regolith. In: Minoglou K, Karafolas N, Cugny B (eds) *International Conference on Space Optics — ICSO 2022*. SPIE, p 230